Binary Planet Formation by Gas-assisted Encounters of Planetary Embryos

Ondřej Chrenko[1] , Miroslav Brož[1] , and David Nesvorný[2]

[1] Institute of Astronomy, Charles University in Prague, V Holešovičkách 2, 18000 Prague 8, Czech Republic; chrenko@sirrah.troja.mff.cuni.cz

[2] Southwest Research Institute, Department of Space Studies, 1050 Walnut Street, Suite 300, Boulder, CO 80302, USA

Abstract

We present radiation hydrodynamic simulations in which binary planets form by close encounters in a system of several super-Earth embryos. The embryos are embedded in a protoplanetary disk consisting of gas and pebbles and evolve in a region where the disk structure supports convergent migration due to Type I torques. As the embryos accrete pebbles, they become heated and thus affected by the thermal torque and the hot-trail effect, which excites orbital eccentricities. Motivated by findings of Eklund & Masset, we assume that the hot-trail effect also operates vertically and reduces the efficiency of inclination damping. Non-zero inclinations allow the embryos to become closely packed and also vertically stirred within the convergence zone. Subsequently, close encounters of two embryos assisted by the disk gravity can form transient binary planets that quickly dissolve. Binary planets with a longer lifetime of $\sim 10^4$ yr form in three-body interactions of a transient pair with one of the remaining embryos. The separation of binary components generally decreases in subsequent encounters and because of pebble accretion until the binary merges, forming a giant planet core. We provide an order-of-magnitude estimate of the expected occurrence rate of binary planets, yielding one binary planet per $\simeq (2-5) \times 10^4$ planetary systems. Therefore, although rare, binary planets may exist in exoplanetary systems and they should be systematically searched for.

Key words: planet–disk interactions – planets and satellites: detection – planets and satellites: dynamical evolution and stability – planets and satellites: formation – planets and satellites: general – protoplanetary disks

Supporting material: animations

1. Introduction

Several classes of celestial objects (e.g., minor solar system bodies, dwarf planets, stars, etc.) are known to exist in binary configurations, i.e., as two bodies orbiting their barycenter, which is located exterior to their physical radii. The existence of binaries is an important observational constraint because a successful population synthesis model for a given class of objects must be able to explain how binaries form, how frequent they are, and how they evolve dynamically and affect their neighborhood.

The richest sample of binary objects within the scope of planetary sciences is in the population of minor solar system bodies. Examples can be found among the near-Earth objects (NEOs; e.g., Margot et al. 2002; Pravec et al. 2006; Scheeres et al. 2006), main-belt asteroids (MBAs; e.g., Marchis et al. 2008; Pravec et al. 2012), Jovian Trojans (e.g., Marchis et al. 2006; Sonnett et al. 2015), and surprisingly frequently among the Kuiper-belt objects (KBOs; e.g., Veillet et al. 2002; Brown et al. 2006; Richardson & Walsh 2006; Noll et al. 2008). Formation of binary minor bodies took place during various epochs of the solar system. Some binary asteroids originated in recent breakup events (Walsh et al. 2008), whereas the binary KBOs were probably established early, during the formation of planetesimals (Goldreich et al. 2002; Nesvorný et al. 2010; Fraser et al. 2017) more than four billion years ago.

For large bodies, the number of binary configurations drops suddenly almost to zero. Of the known and confirmed objects, only Pluto and Charon can be considered as a binary (Christy & Harrington 1978; Walker 1980; Lee & Peale 2006; Brozović et al. 2015), likely of an impact origin (Canup 2011; McKinnon et al. 2017). Since Pluto and Charon were classified as *dwarf*

planets, the conclusion stands that no planets in binary configurations have yet been discovered.

Given that more than 3700 exoplanets have been confirmed to date,[3] the paucity of binary planets is a well-established characteristic of the data set. However, its implications for our understanding of planet formation are unclear and maybe even underrated at present. Are binary planets scarce, and is it just that current methods preclude their discovery? Or is their non-existence a universal feature shared by all planetary systems throughout the Galaxy?

To start addressing these questions, this paper discusses the formation of binary planets by two- and three-body encounters of planetary embryos in protoplanetary disks, during the phase when the gas is still abundant and the embryos still grow by pebble accretion (Ormel & Klahr 2010; Lambrechts & Johansen 2012). We advocate that suitable conditions to form binary planets are achieved when orbital eccentricities and inclinations or embryos are excited by thermal torques related to accretion heating (Chrenko et al. 2017; Eklund & Masset 2017). Our model utilizes radiation hydrodynamics (RHD) to account for these effects.

Although the results of this paper are preliminary in many aspects, they demonstrate that binary planets can exist and it may be only a matter of time (or advancements in methods) before such an object is discovered in one of the exoplanet search campaigns. To motivate future observations and data mining, we emphasize that promising methods for detections of exomoons have been developed and applied in recent years. These include, for example, transit timing variations (TTVs; Simon et al. 2007) and transit duration variations (TDVs;

---

[3] As of 2018 August, according to the NASA Exoplanet Archive: https://exoplanetarchive.ipac.caltech.edu/.

Kipping 2009), their Bayesian analysis in the framework of direct star–planet–moon modeling and fitting (Kipping et al. 2012), photometric analysis of phase-folded light curves using the scatter peak (SP) method (Simon et al. 2012) or the orbital sampling effect (OSE; Heller 2014; Hippke 2015), microlensing events (Han 2008; Liebig & Wambsganss 2010; Bennett et al. 2014), and asymmetric light curves due to plasma tori of hypothetical volcanic moons (Ben-Jaffel & Ballester 2014).

Indeed, Kepler-1625 b-i has recently been identified as an exomoon candidate (Heller 2018; Teachey et al. 2018) and is awaiting a conclusive confirmation. Moreover, Lewis et al. (2015) discuss that the *CoRoT* target SRc01 E2 1066 can be explained as a binary gas-giant planet, although the signal could also correspond to a single planet transiting a starspot (Erikson et al. 2012). Therefore, methods similar to those listed above could be applicable when searching for binary planets.

Our paper is organized as follows. In Section 2, we outline our RHD model. Section 3 describes our nominal simulation with the formation of binary planets. Planetary encounters are analyzed, as well as the influence of the gas disk. Subsequently, we test the stability of binary planets in several simplified models (without neighboring embryos; without the disk; etc.). We also study binary planet formation in a set of four additional simulations to verify the relevance of the process. In Section 4, we estimate the expected occurrence rate of binary planets in the exoplanetary population and we also discuss a possible role of binary planets in planetary sciences. Section 5 is devoted to conclusions.

1.1. Definitions

To avoid confusion, let us list several definitions that we use throughout the rest of the paper.

1. *Binary* is shorthand for a binary planet, not to be mistaken with binary stars etc.
2. *Transient* (also *transient binary* or *transient pair*) is a binary that forms by two-body encounters of planetary embryos (e.g., Astakhov et al. 2005), in our case with the assistance of the disk gravity as we shall demonstrate later. We choose the name *transient* because we find the typical lifetime of these binaries to be of the order of one stellarcentric orbital period.
3. *Hardening* (e.g., Hills 1975) is a process during which the orbital energy of a binary configuration is dissipated and the separation of binary components decreases.
4. *Stability* of a binary planet is discussed if it can survive more than one stellarcentric orbital period, which is usual after hardening. In principle, such a binary can be observed. We characterize *stability* by means of the lifetime over which the binary components remain gravitationally bound.
5. *Encounter* refers to a close encounter of two or more planetary embryos (single or binary), when they enter one another's Hill sphere.
6. *Merger* refers to a physical collision of two embryos. In our approximation, we replace the colliding embryos by a single object, assuming perfect merger (mass and momentum conservation).
7. We denote orbital elements in the stellarcentric frame with a subscript "s" to distinguish them from the orbital elements of one binary component with respect to another

(e.g., a_s is the stellarcentric semimajor axis but a is the semimajor axis of the binary configuration).

2. Radiation Hydrodynamic Model

2.1. General Overview

The individual constituents of our model are as follows. First, we consider radiation transfer, which is essential to properly reproduce the disk structure (Bitsch et al. 2013) and to account for all components of the Type I torque acting on low-mass planets (e.g., Baruteau & Masset 2008; Kley & Crida 2008; Kley et al. 2009; Lega et al. 2014).

Second, we use a two-fluid approximation to include a disk of pebbles, which serves as a material reservoir for the accreting embryos (Ormel & Klahr 2010; Lambrechts & Johansen 2012; Morbidelli & Nesvorný 2012).

Third, we also take into account that pebbles heat the accreting embryos, which in turn heat the gas in their vicinity. The migration is then modified due to the thermal torque (Benéz-Llambay et al. 2015; Masset 2017) and its dynamical component—the hot-trail effect (Chrenko et al. 2017; Eklund & Masset 2017; Masset & Velasco Romero 2017)—which perturbs the embryos in such a way that their orbital eccentricities are excited. This is due to the epicyclic motion of the embryo, which causes variations in the azimuthally uneven distribution of the heated (and thus underdense) gas.

The numerical modeling is done with the FARGO_THORIN code[4], which was introduced and described in detail in Chrenko et al. (2017). The code is based on FARGO (Masset 2000). The model is 2D (vertically averaged) but planets are evolved in 3D. A number of important vertical phenomena were implemented, although some with unavoidable approximations.

A new phenomenon implemented in this study is the vertical hot-trail effect described by Eklund & Masset (2017), which can excite orbital inclinations. Such excitation should not occur for an isolated and non-inclined orbit because it is quenched by the growth in eccentricity, which is faster (Eklund & Masset 2017); however, the vertical hot-trail effect operates when a non-negligible inclination is initially excited by some other mechanism. For example, it can become important in a system of multiple embryos where close encounters temporarily pump up the inclinations. The vertical hot trail then starts to counteract the usual inclination damping by bending waves (Tanaka & Ward 2004).

2.2. Governing Equations

Gas is treated as a viscous Eulerian fluid described by the surface density Σ, flow velocity $\boldsymbol{v}$ on the polar staggered mesh, and the internal energy ϵ. The pebble disk is represented by an inviscid and pressureless fluid with its own surface density Σ_p and velocity $\boldsymbol{u}$. We assume two-way coupling between the two fluids by linear drag terms, with the Stokes number τ calculated for the Epstein regime.

The RHD partial differential equations read

$$\frac{\partial \Sigma}{\partial t} + \nabla \cdot (\Sigma \boldsymbol{v}) = 0, \qquad (1)$$

---

[4] The code is available at http://sirrah.troja.mff.cuni.cz/~chrenko.

$$\frac{\partial \boldsymbol{v}}{\partial t} + \boldsymbol{v} \cdot \nabla \boldsymbol{v} = -\frac{1}{\Sigma}\nabla P + \frac{1}{\Sigma}\nabla \cdot \overset{\leftrightarrow}{T} - \frac{\int \rho \nabla \phi \, dz}{\Sigma} + \frac{\Sigma_{\mathrm{p}}}{\Sigma}\frac{\Omega_{\mathrm{K}}}{\tau}(\boldsymbol{u} - \boldsymbol{v}), \tag{2}$$

$$\frac{\partial \epsilon}{\partial t} + \nabla \cdot (\epsilon \boldsymbol{v}) = -P\nabla \cdot \boldsymbol{v} + Q_{\mathrm{visc}} + Q_{\mathrm{acc}} + \frac{2\sigma_{\mathrm{B}}}{\tau_{\mathrm{eff}}}(T_{\mathrm{irr}}^4 - T^4) - 2H\nabla \cdot \boldsymbol{F}, \tag{3}$$

$$\frac{\partial \Sigma_{\mathrm{p}}}{\partial t} + \nabla \cdot (\Sigma_{\mathrm{p}}\boldsymbol{u}) = -\left(\frac{\partial \Sigma_{\mathrm{p}}}{\partial t}\right)_{\mathrm{acc}}, \tag{4}$$

$$\frac{\partial \boldsymbol{u}}{\partial t} + \boldsymbol{u} \cdot \nabla \boldsymbol{u} = -\frac{\int \rho_{\mathrm{p}} \nabla \phi \, dz}{\Sigma_{\mathrm{p}}} - \frac{\Omega_{\mathrm{K}}}{\tau}(\boldsymbol{u} - \boldsymbol{v}), \tag{5}$$

where the individual quantities are the pressure P, viscous stress tensor $\overset{\leftrightarrow}{T}$ (e.g., Masset 2002), gas volume density ρ, volume density of pebbles ρ_{p}, coordinate z perpendicular to the midplane, gravitational potential ϕ of the primary and the planets, Keplerian angular frequency Ω_{K}, viscous heating term Q_{visc} (Mihalas & Weibel Mihalas 1984), accretion heating term Q_{acc} related to the accretion sink term $(\partial \Sigma_{\mathrm{p}}/\partial t)_{\mathrm{acc}}$, Stefan–Boltzmann constant σ_{B}, effective vertical optical depth τ_{eff} (Hubeny 1990), irradiation temperature T_{irr} (Chiang & Goldreich 1997; Menou & Goodman 2004; Baillié & Charnoz 2014), midplane gas temperature T (the term $\propto T^4$ describes vertical cooling), vertical pressure scale height H, and radiative flux $\boldsymbol{F}$.

The ideal-gas state equation is used as the thermodynamic closing relation:

$$P = (\gamma - 1)\epsilon = \Sigma \frac{R}{\mu} T, \tag{6}$$

where γ is the adiabatic index, R is the universal gas constant, and μ is the mean molecular weight. Equation (6) has been widely used in numerical models to relax inferior isothermal approximations and to account for the disk thermodynamics (through the energy equation), which is important for accurate migration rates (e.g., Kley & Crida 2008; Kley et al. 2009; Lega et al. 2014). We also point out that the given state equation neglects the radiation pressure and phase transitions, which is a valid assumption in low-temperature disks (D'Angelo et al. 2003).

Finally, flux-limited diffusion and the one-temperature approximation are utilized to describe the in-plane radiation transport, leading to

$$\boldsymbol{F} = -D\nabla T = -\lambda_{\mathrm{lim}}\frac{16\sigma_{\mathrm{B}}T^3}{\rho_0 \kappa}\nabla T, \tag{7}$$

where D denotes the diffusion coefficient, λ_{lim} is the flux limiter according to Kley (1989), ρ_0 is the midplane volume density, and $\kappa(\rho, T)$ is the material opacity. We use the opacity by Bell & Lin (1994) for both the Rosseland and Planck opacities.

For completeness, we provide the accretion heating formula

$$Q_{\mathrm{acc}} = \sum_i \frac{GM_{\mathrm{em},i}\dot{M}_{\mathrm{em},i}}{R_i S_{\mathrm{cell}}}, \tag{8}$$

where the sum goes over all embryos with indices i, masses $M_{\mathrm{em},i}$, self-consistently calculated pebble accretion rates $\dot{M}_{\mathrm{em},i}$, and physical radii R_i. G is the gravitational constant and S_{cell} is the surface area of the cell that contains the respective embryo and in which the heat is liberated (Q_{acc} is zero in other cells).

2.3. Evolution of Planets and Inclination Damping

Planets are evolved on 3D orbits using the IAS15 integrator (Rein & Liu 2012; Rein & Spiegel 2015). Planetary collisions are treated as perfect mergers. The planet–disk interactions are calculated by means of the vertical averaging procedure of Müller et al. (2012). The planetary potential is adopted from Klahr & Kley (2006) and has the smoothing length $r_{\mathrm{sm}} = 0.5R_{\mathrm{H}}$, where R_{H} is the planet's Hill sphere.

When computing the torque acting on an embryo, we do not exclude any part of the Hill sphere because we focus on low-mass embryos (Lega et al. 2014). Such an exclusion is required only when embryos exceed masses $\simeq 10\,M_{\oplus}$ and form a circumplanetary disk. This disk should not contribute to the gas-driven torque because it comoves with the embryo (Crida et al. 2008). Our model ignores the torques from pebbles (Benéz-Llambay & Pessah 2018) because we assume relatively low pebble-to-gas mass ratios (less than 0.001). But we point out that during accretion of pebbles, we account for the transfer of their mass and linear momentum onto the embryo.

An important ingredient when investigating 3D planetary orbits is the inclination damping (e.g., Cresswell et al. 2007). We include the damping by using the formula from Tanaka & Ward (2004). In our case, the damping acceleration perpendicular to the disk plane reads

$$a_z = \begin{cases} \beta\dfrac{\Sigma\Omega_{\mathrm{K}}}{c_{\mathrm{s}}^4}(2A_z^c v_z + A_z^s z\Omega_{\mathrm{K}}), & I > I_0 \\ 0, & I \leqslant I_0 \end{cases} \tag{9}$$

where $\beta = 0.3$ (e.g., Pierens et al. 2013), $A_z^c = -1.088$, and $A_z^s = -0.871$ are fixed coefficients, c_{s} is the sound speed, v_z is the embryo's vertical velocity, and z is its vertical separation from the midplane. Σ and Ω_{K} are evaluated along the embryo's orbit.

In writing Equation (9), we introduce a simple modification of Tanaka & Ward's formula. We assume that the inclination damping does not operate when the orbital inclination I is below a certain critical value I_0. The motivation for this modification stems from the findings of Eklund & Masset (2017), who investigated the orbital evolution of a hot (accreting) planet in a 3D radiative disk. Not only did they find the excitation of the eccentricity due to the hot-trail effect, but they also showed that the effect has a vertical component that can excite the inclinations.

In our 2D model with accretion heating, the excitation of eccentricity is reproduced naturally. Regarding the inclinations, we simply assume that the hot-trail effect operates vertically as well and balances the inclination damping up to the value I_0. For larger inclinations, the damping takes over and the standard formula for a_z applies. We consider I_0 to be a free parameter of
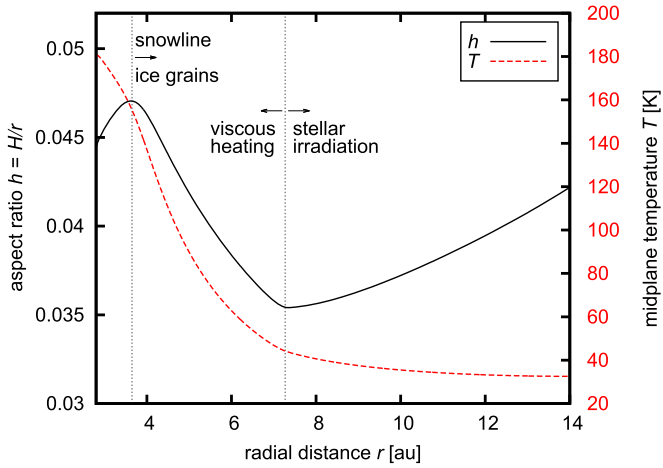
Figure 1. Radial profile of the aspect ratio $h(r) = H/r$ and temperature $T(r)$ in the disk used in our simulations. The right vertical dotted line marks the transition between the viscously heated and stellar irradiated regions, the latter exhibiting flaring of the disk. The left vertical dotted line corresponds to the water ice line, which is also a local maximum of the opacities of Bell & Lin (1994). The figure is taken from Chrenko et al. (2017).

the model and choose $I_0 = 10^{-3}$ rad $\simeq 0°057$, which is at the lower end of the results of Eklund & Masset (2017).

3. Simulations

3.1. Disk Model

The protoplanetary disk model used in all our RHD simulations is exactly the same as in Chrenko et al. (2017), including the initial and boundary conditions (de Val-Borro et al. 2006). The parameters[5] characterizing the initial gas disk are the surface density $\Sigma = 750(r/(1\,\mathrm{au}))^{-0.5}$ g cm^{-2}, kinematic viscosity $\nu = 5 \times 10^{14}$ cm^2 s^{-1}, adiabatic index $\gamma = 1.4$, mean molecular weight $\mu = 2.4$ g mol^{-1}, vertical opacity drop $c_\kappa = 0.6$, and disk albedo $A = 0.5$. The central star has an effective temperature $T_\star = 4370$ K, stellar radius $R_\star = 1.5\,R_\odot$, and mass $M_\star = 1\,M_\odot$. The domain stretches from $r_{\min} = 2.8$ au to $r_{\max} = 14$ au in radius and spans the entire azimuth, having a grid resolution of 1024×1536 (rings $\times$ sectors).

The gas disk is numerically evolved to its thermal equilibrium and only after that is the coupled pebble disk introduced. Pebbles are parameterized by the radial pebble mass flux $\dot{M}_F = 2 \times 10^{-4}\,M_\oplus$ yr^{-1} (Lambrechts & Johansen 2014), the Schmidt number $Sc = 1$, coagulation efficiency $\epsilon_p = 0.5$ (Lambrechts & Johansen 2014), bulk density $\rho_b = 1$ g cm^{-3}, and turbulent stirring efficiency $\alpha_p = 1 \times 10^{-4}$ (e.g., Youdin & Lithwick 2007). To infer the pebble sizes, we assume the drift-limited growth regime (Birnstiel et al. 2012; Lambrechts & Johansen 2014), leading to pebble sizes of several centimeters.

For reference, Figure 1 shows the radial profiles of the aspect ratio $h(r) = H/r$ and temperature $T(r)$ of the equilibrium gas disk. The $h(r)$ profile has a maximum near 4 au, where the opacity peaks just before the sublimation of water ice (Bell & Lin 1994). Therefore the heat produced by viscous heating is not easily radiated away from this opaque region and the disk puffs up.

Near 7 au, the disk starts to flare because the vertical optical depth is small enough for the incoming radiation to penetrate

deeper and heat the disk. The transition to the flared outer parts produces a zone of convergent Type I migration for planetary embryos (Bitsch et al. 2013; Pierens 2015).

3.2. Nominal Simulation

Let us now discuss and analyze our nominal simulation in which binary planets were found to form. Initially, we set four embryos on circular orbits with stellarcentric semimajor axes $a_s = 5, 6.7, 8.4,$ and 10.1 au, inclinations $I_s = I_0 = 10^{-3}$ rad $\simeq 0°057$, and randomized longitudes. The initial mass of each embryo is $M_{\rm em} = 3\,M_\oplus$ and their orbital separations are equal to 16 mutual Hill radii:

$$R_{{\rm mH},ij} = \frac{a_{s,i} + a_{s,j}}{2}\left(\frac{M_{{\rm em},i} + M_{{\rm em},j}}{3M_\star}\right)^{1/3}. \qquad (10)$$

Embryos are numbered 1, 2, 3, and 4 from the innermost outward.

Figure 2 shows the evolution of embryos over 140 kyr of the full RHD simulation with pebble accretion and respective heating. At first, the embryos undergo convergent migration toward their zero-torque radius. Without the heating torques, the embryos would concentrate near 7 au thanks to the contribution of the entropy-related corotation torque (Paardekooper & Mellema 2008), which is positive from $\simeq$4 to 7 au in this particular disk model.

With the heating torques, however, the zero-torque radius is shifted further out because these torques are always positive (Benéz-Llambay et al. 2015). Moreover, the hot-trail effect quickly excites orbital eccentricities. Within $\simeq$2 kyr, the eccentricities reach $e_s \simeq 0.02$ for the innermost embryo and $e_s \simeq 0.04$ for the outermost.

The inclinations first remain constant near the prescribed I_0 value, with only small temporal excitations not exceeding $I_s \simeq 0°2$. Even these initially small inclinations are enough to modify the encounter geometries in such a way that the system becomes gradually stirred in the vertical direction. Once the system becomes closely packed, at about $\simeq$35 kyr into the simulation, the mutual close encounters pump the inclinations significantly, typically to $I_s \simeq 1°$ and even up to $I_s \simeq 2°$. Planets can pass above or below each other because their vertical excursions are comparable to (or larger than) their Hill spheres. For example, the maximal vertical excursion of a $5\,M_\oplus$ embryo at 10 au is $z_{\max} \simeq 2R_H$ when $I_s = 2°$.

Due to excited eccentricities, the embryos never form a stable resonant chain, in accordance with Chrenko et al. (2017). Moreover, the excited inclinations help the embryos to avoid collisions and mergers for a long period of time. Consequently, close encounters of embryos are frequent in the system. Between $\simeq$98 kyr and $\simeq$114 kyr, strong unphysical oscillations of the stellarcentric orbital elements appear in Figure 2 for some of the embryos, indicating formation of gravitationally bound binary planets.[6]

---

[5] A great number of the parameters listed in this section (ν, c_κ, A, $T_\star$, $R_\star$, $\dot{M}_F$, Sc, ϵ_p, ρ_b, α_p) were not defined in Section 2 to keep it brief. To understand how these parameters enter the model, we refer the reader to Chrenko et al. (2017).

[6] In Figure 2, we can also identify co-orbital configurations (1/1 resonances), for example for embryos 1 and 3 between 62.5 and 66 kyr. To keep the paper focused on binary planets, we refer the interested reader to other works discussing formation and detectability of co-orbital planets, e.g., Laughlin & Chambers (2002), Cresswell & Nelson (2008), Giuppone et al. (2012), Chrenko et al. (2017), Brož et al. (2018).
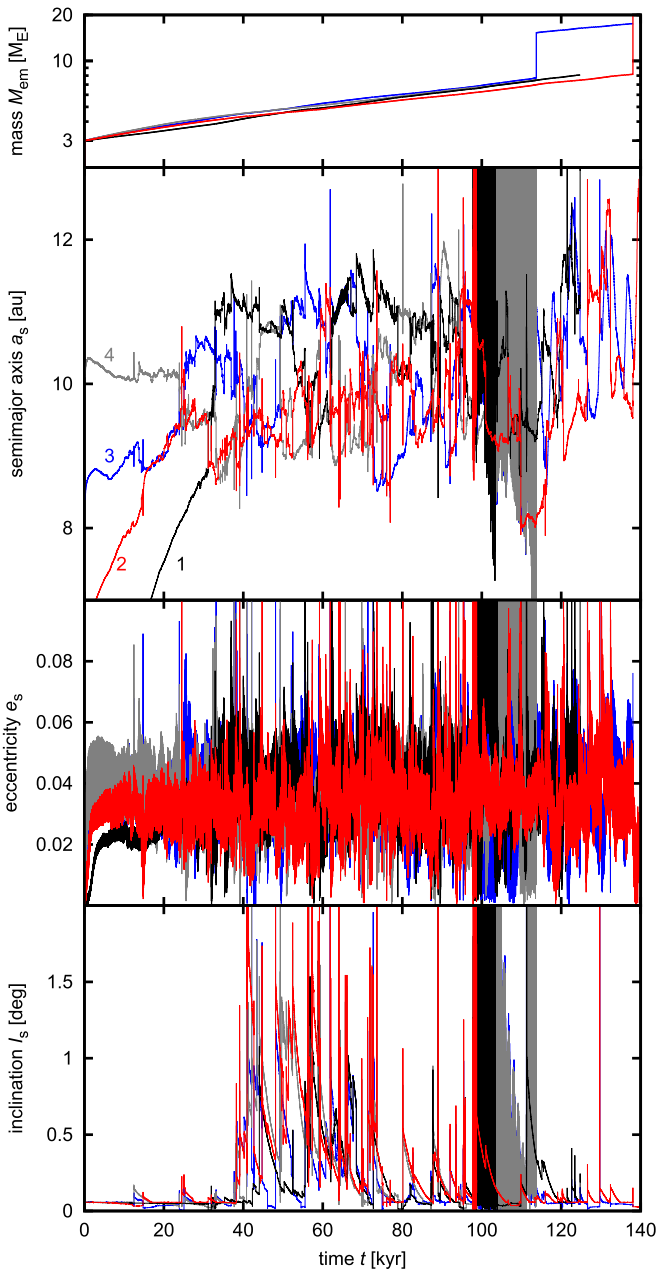
Figure 2. Temporal evolution of the embryo masses M_{em} (top), stellarcentric semimajor axes a_s (second row), eccentricities e_s (third row), and inclinations I_s (bottom) in the full RHD simulation with the gas disk, pebble disk, pebble accretion, and accretion heating. Initially, there are four migrating embryos, numbered from the innermost outward. The inclination starts at $I_0 = 10^{-3}$ rad; the inclination damping is switched off whenever $I \leqslant I_0$. The strong variations of the stellarcentric Keplerian elements between $\simeq 98$ kyr and $\simeq 114$ kyr are a consequence of binary planet formation. A member of the binary swaps for one of the accompanying embryos three times, as indicated by the change in color of the oscillating curves (from a narrow strip of red to black and to gray). The existence of the binary is ended abruptly by a merger (clearly related to the instantaneous mass increase in the $M_{em}(t)$ plot).

3.3. Gravitationally Bound Pairs of Embryos

To identify the events related to the binary formation in the simulation described above, we computed orbits of the relative motion among all possible pairs of embryos and selected those with $a < R_{mH}$, $e < 1$. The results are shown in Figure 3. Throughout the simulation, we found 65 time intervals during which at least two embryos are captured on a mutual elliptical
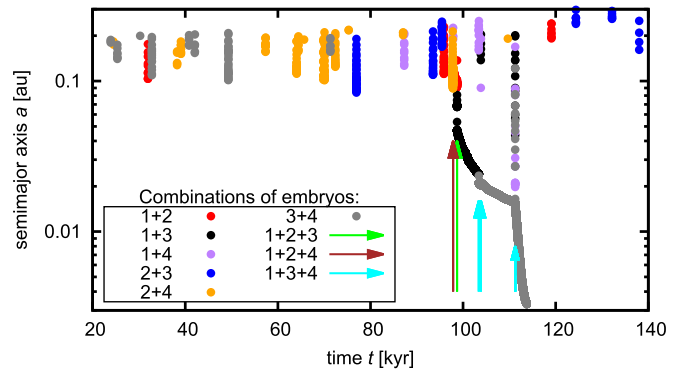
Figure 3. The record of all relative two-body orbits satisfying the conditions $a < R_{mH}$ and $e < 1$ in our nominal simulation. The filled circles mark the instantaneous semimajor axes and each pair of embryos is distinguished by color. The arrows are used to indicate when a gravitationally bound pair participates in a three-body encounter.

orbit, changing their relative orbital energy from initially positive to negative (and back to positive when the capture terminates). Subsequently, we also scanned the sample of bound pairs and looked for cases when a third embryo has its distance from a pair $d < R_{mH}$ to identify three-body (pair–embryo) encounters. These are highlighted in Figure 3 by arrows.

Analyzing the lifetime of the bound pairs, we found that most of them dissolve before finishing one stellarcentric orbit. However, we found a single case when several binary configurations existed consecutively for a prolonged period of time between $\simeq 98$ kyr and $\simeq 114$ kyr. This time interval is bordered by three-body encounters, which usually cause the binary separation to drop.

In summary, bound pairs can form in two-body encounters but they quickly dissolve unless they undergo a three-body encounter with one of the remaining embryos. The latter process is known as binary hardening (e.g., Hills 1975, 1990; Goldreich et al. 2002; Astakhov et al. 2005) and it occurs when an external perturber removes energy from a binary system, which then becomes more tightly bound. To distinguish between two types of events contributing to the formation of bound pairs, we call those formed in two-body encounters *transient* binaries because of their typically short dynamical lifetime.

Transient binaries have been the subject of many different studies, for example, in the three-body Hill problem (e.g., Simó & Stuchi 2000; Astakhov et al. 2005). Their formation is possible because the orbital energy of two bodies in no longer conserved when additional perturbers (e.g., the central star) are present (e.g., Cordeiro et al. 1999; Araujo et al. 2008). Our system is of course more complicated because additional gravitational perturbations arise from the gas disk. We will demonstrate in Section 3.4 that the gas indeed facilitates formation of transients.

One last question we address here is whether or not the occurrence of bound pairs in Figure 3 is related to the vertically stirred orbits of embryos. To find an answer, we looked for bound pairs (with $a < R_{mH}$, $e < 1$) in one of our previous simulations reported in Chrenko et al. (2017) (dubbed Case III), where the inclinations were damped in the standard way (Tanaka & Ward 2004). We found only six bound pairs (all transients) compared to 65 cases in our nominal simulation presented here. Therefore, the excited inclinations importantly

Chrenko, Brož, & Nesvorný
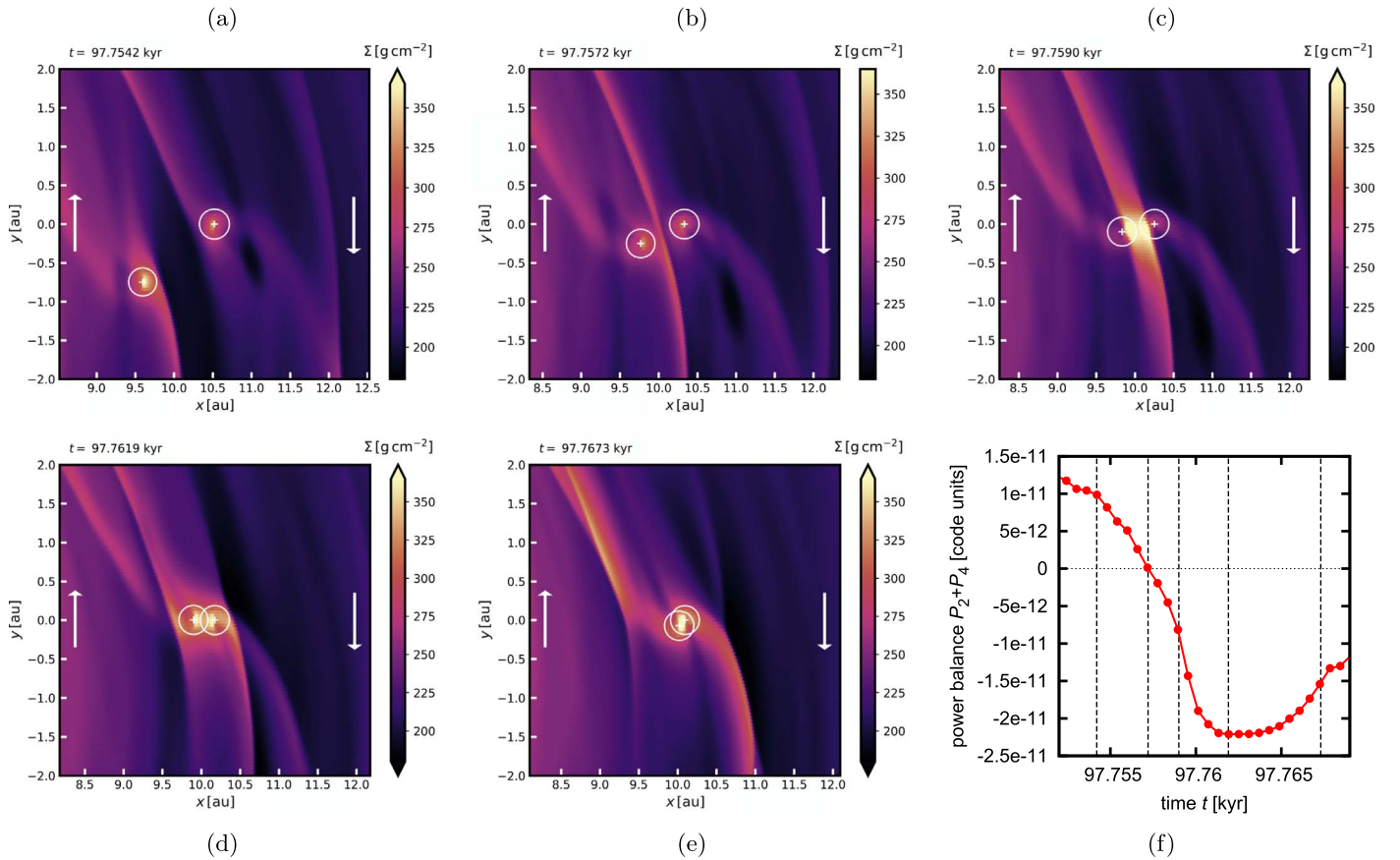
Figure 4. Formation of a transient binary during a two-body encounter of embryos 2 and 4. The first five panels (a)–(e) show the evolution of the perturbed surface gas density Σ. Locations of the embryos are marked by white crosses, their Hill spheres are indicated by white circles, and white arrows show the direction of the Keplerian shear in the reference frame corotating with embryo 2, which is placed at the center of each plot. The individual panels are labeled with the simulation time t. The final panel (f) shows the evolution of the total power of the gravitational forces exerted by the disk on embryos 2 and 4. The vertical dashed lines mark the simulation time corresponding to the snapshots of Σ in panels (a)–(e). An animation of the formation of the transient binary is available in the online Journal and covers $t \simeq 97.73$–97.8 kyr in simulation time.

(An animation of this figure is available.)

change the outcomes of embryo encounters in the gas disk and help to form transients.

3.4. Transient Binary Formation in a Two-body Encounter

Here we investigate the formation of a transient pair of embryos 2 and 4, which precedes the binary hardening events in our nominal simulation. The pair forms in a two-body interaction at $t \simeq 97.76$ kyr. To see whether the embryo–disk interactions assist in the process, we show in Figure 4 the evolution of the perturbed gas surface density Σ during the encounter.

Before the encounter (panel (a)), the usual structures can be seen in the disk. The hot (underdense) trail of the outer embryo 2 can be seen as a dark oval spot in the bottom right quadrant (it moves down and gets larger in time). The hot trail of the inner embryo 4 is less prominent and looks like an underdense gap attached to the embryo from inside.

As the embryos approach in panel (b), the outer spiral arm of the inner embryo 4 and the inner spiral arm of the outer embryo 2 join and overlap. The overlap forms a strong density wave positioned between the embryos. The overdensity increases as part of the wave becomes trapped between the Hill spheres of the two embryos in panel (c). From panel (c) to (d), the embryos cross this shared density wave.

In panel (d), the embryos are so close to each other that they effectively act on the disk as a single mass, and the previously shared spiral arm splits into an inner and an outer component with a small pitch angle. There are two more spirals with a larger pitch angle that are leftovers of the initial wakes launched by the embryos. In panel (e), all spirals blend into a single pair of arms. The embryos enter one another's Hill sphere between panels (d) and (e) through the vicinity of the Lagrange points L_1 for the outer and L_2 for the inner embryo (Astakhov et al. 2005). The embryos are captured on a prograde binary orbit (in panel (e), embryo 4 orbits the central embryo 2 counterclockwise).

The spiral arm crossing that appears during the encounter is known to produce strong damping effects on the embryos (Papaloizou & Larwood 2000). It is thus likely that the gas supports the gravitational capture by dissipating the orbital energy. To quantify this effect, we measured the total gravitational force $\boldsymbol{F}_{g,i}$ exerted by the disk on each embryo and we calculated the mechanical power

$$P_i = \int_{\text{disk}} \boldsymbol{v}_i \cdot \boldsymbol{F}_{g,i} dS, \qquad (11)$$

where $\boldsymbol{v}_i$ is the velocity vector of the embryo and the integral goes over the entire disk. P_i directly determines the rate of

6

change of the orbital energy $\dot{E}_i$ of each embryo (e.g., Cresswell et al. 2007).

Panel (f) of Figure 4 shows the total balance of the energy subtraction (or addition) for embryos 2 and 4, $P = P_2 + P_4$. The energy is transferred to the disk when $P < 0$ and subtracted from the disk when $P > 0$. It is obvious that throughout the closest approach (panels (b)–(e)), the orbital energy of the embryos dissipates and thus the influence of the gas disk on the formation of transients is confirmed.

3.5. Binary Planet Hardening in Three-body Encounters

The transient pair of embryos 2 and 4 does not dissolve; instead it is further stabilized in three-body encounters with the remaining embryos. Figure 5 shows these encounters in detail. First, the transient pair encounters embryo 1 at $t \simeq 97.85$ kyr. During this encounter, one component of the binary (embryo 4) becomes unbound and is deflected away, but the incoming embryo 1 takes its place in an exchange reaction so the binary continues to exist.

Similar situations occur at about $\simeq 98.69$ kyr, when the configuration $1 + 2$ changes to $1 + 3$, and at $\simeq 103.4$ kyr, when the configuration $1 + 3$ changes to $3 + 4$. Figure 5 also reveals that the binary becomes hardened with each encounter since the overlap between the $r(t)$ curves for the binary components becomes tighter.

An even clearer indication of binary hardening is provided by Figure 6, where we plot the temporal evolution of the orbital elements of the binary planet. The color of the curves changes each time there is a change in the composition of the binary. One can further notice that the exchange interactions produce sudden decreases of a and also of e. Between the exchange interactions, a decreases smoothly whereas e generally increases in an oscillatory manner. We will describe these variations later.

Considering the binary planet inclination, the transient binary $2 + 4$ forms with a prograde orbit and a relatively low inclination. During the first three-body encounter, the binary is reconfigured to a retrograde orbit with the inclination oscillating between $100°$ and $170°$. The inclination then slowly evolves toward $180°$ regardless of the swap encounters, which only diminish the amplitude of the oscillation.

The binary planet does not survive to the end of our simulation. At $\simeq 111.26$ kyr, it undergoes a three-body exchange interaction with embryo 1 during which their Hill spheres overlap for a prolonged period of time (see the spike in Figure 3 at $\simeq 111.26$ kyr). Consequently, the binary inclination is flipped from the retrograde configuration to $I = 80°$. In this configuration, the binary undergoes a fast decrease of a, accompanied by an equally fast increase of e. Consequently, the binary planet ends its life in a merger into a single body.

3.6. Binary Planet Evolution without Perturbing Embryos

The lifetime of the hardened binary in our nominal simulation is long enough ($\sim 10^4$ yr) to be interesting. There are two basic questions that we shall now address. First, what is the evolution of such a binary if the surrounding embryos and their perturbations are ignored? And second, what causes the changes in the binary orbital elements between the three-body encounters in Figure 6?

To answer these questions, we discard the non-binary embryos and restart the simulation from the configuration of

the binary planet,[7] gas, and pebbles corresponding to $t = 100$ kyr. Three models are numerically evolved for 45 kyr. The first one has the same setup as the initial simulation (apart from the ignored non-binary embryos). In the second one, the accretion heating is disabled but the mass of the binary components can still grow by pebble accretion. In the third one, we again switch off accretion heating and discard the pebble disk; the binary mass therefore remains constant.

The orbital evolution of the binary in these three cases is shown in Figure 7. The evolution of the inclination is more or less the same, regardless of the model, and converges toward a fully retrograde configuration. The semimajor axis decreases as a consequence of pebble accretion, which transports the linear momentum and mass onto the binary components, thus changing their orbital angular momentum. It is worth noting that if the pebble accretion and accretion heating are ignored, the isolated binary planet evolving in the radiative disk exhibits only minor orbital changes (once it adjusts to the removal of the surrounding embryos at the beginning of the restart).

The eccentricity substantially changes only in the model with accretion heating, otherwise it oscillates around its initial value or exhibits a slow secular variation. In other words, not only is the hot-trail effect important for exciting the eccentricities of individual embryos before the encounter phase, but it is also responsible for pumping the eccentricity of the binary up to an asymptotic value $e \simeq 0.75$.

These findings justify our incorporation of pebble accretion and accretion heating into the model because both phenomena affect the rate of change of the binary orbital elements. Pebble accretion diminishes the semimajor axis and accretion heating excites the eccentricity.

3.7. Binary Planet Evolution in the Disk-free Phase

When protoplanetary disks undergo dispersal due to photoevaporation, the emerging planetary systems may become unstable (e.g., Lega et al. 2013). Here we test whether the hardened binary planet could survive the gas removal phase and the subsequent orbital instabilities. Since the binary undergoes three-body encounters during the disk phase, they can also be expected after removal of the disk.

To investigate the evolution after the photoevaporation, we remove the fluid part of the model (i.e., gas and pebbles) instantly and continue with a pure N-body simulation. The orbits are integrated for an additional 10 Myr. To account for the chaotic nature of an N-body system with close encounters, we extract 48 orbital configurations of the embryos from between $\simeq 99.7$ kyr and $\simeq 102.4$ kyr of the nominal simulation and use them as the initial conditions for 48 independent integrations.

Our aim is to quantify the survival rate of binary planets. Figure 8 shows the evolution of the fraction N_{surv}/N_{tot}, where N_{surv} is the number of N-body systems still containing a binary planet at simulation time t and N_{tot} is the total number of systems (48). The dependence exhibits a steep decrease—the binary dissolves before 0.1 Myr of evolution in $\simeq 45\%$ of cases and before 1 Myr in $\simeq 76\%$ of cases. However, the trend for $t \geqslant 1$ Myr becomes rather flat. The binary planet survives the whole integration timespan in 15% of our runs.

---

[7] The binary elements at the moment of restart are $a \simeq 0.035$ au, $e \simeq 0.66$, $I \simeq 2.6$ rad.
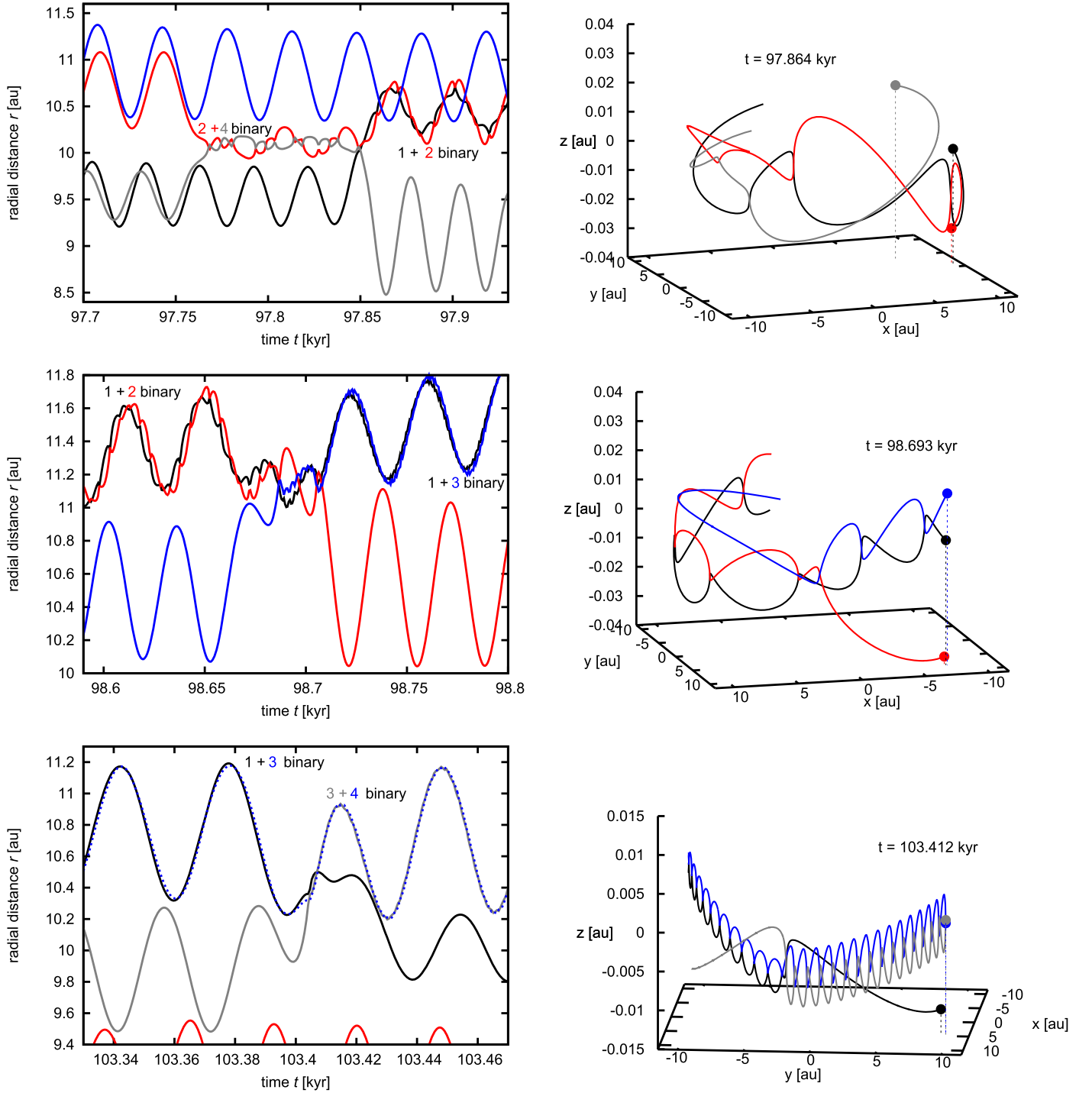
Figure 5. Details of important three-body encounters occurring in the nominal simulation, leading to reconfiguration and hardening of the binary planet. Each row shows a different encounter (and the first row also shows the transient binary of embryos 2 + 4 preceding the three-body encounters). We plot the temporal evolution of the radial distance r (left column) and also the orbital evolution in 3D Cartesian space (right column) in a short time interval around the respective encounters. The numbering and coloring of the bodies is the same as in Figure 2. Filled circles in the right column mark the positions of embryos at the simulation time t given by the labels. An animated version of the top row of Figure 5 is available in the online Journal. The animation spans $t \simeq$ 97.7–97.92 kyr in simulation time, displaying the same tracks as in the static figure.

(An animation of this figure is available.)

We estimate the fraction of planetary systems f_{surv} in which the binary can survive the orbital instabilities. An estimate for young systems can be readily made by taking the final fraction of our integrations conserving the binary, yielding $f_{surv,10\,Myr} \simeq 15\%$. To make an estimate for older systems, we performed a power-law extrapolation of the flat tail of the distribution in Figure 8. The resulting extrapolation $0.22(t/(1\,Myr))^{-0.21}$ yields $f_{surv,4.5\,Gyr} \simeq 4\%$ for $t = 4.5$ Gyr (i.e., comparable to the age of the solar system).

Let us briefly discuss the orbital architecture of the individual systems at the end of our integrations (Figure 9). The systems that retained the binary can be divided into two
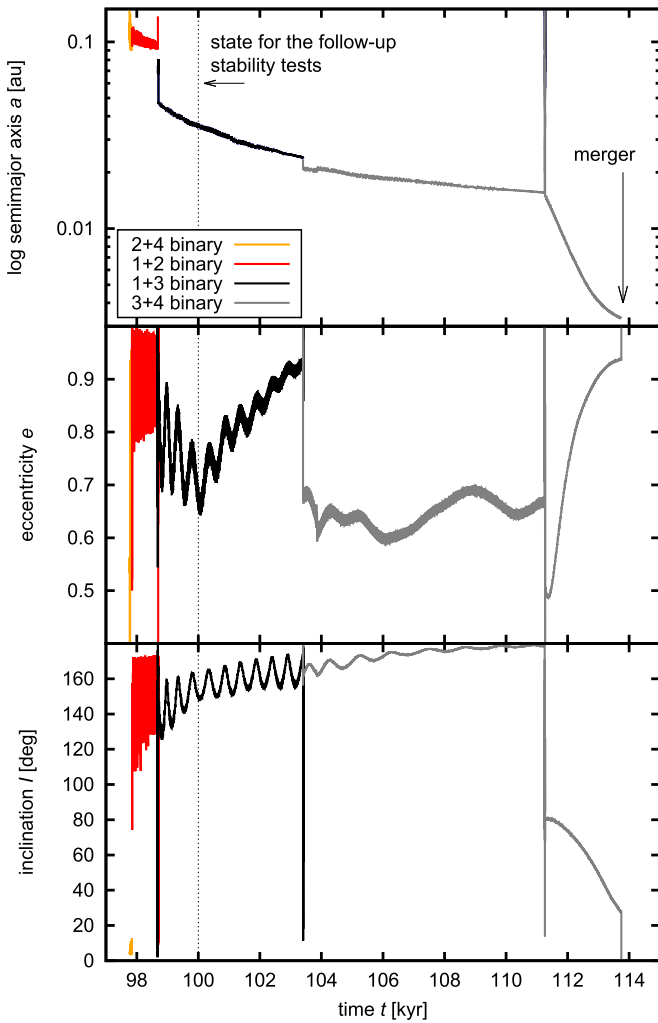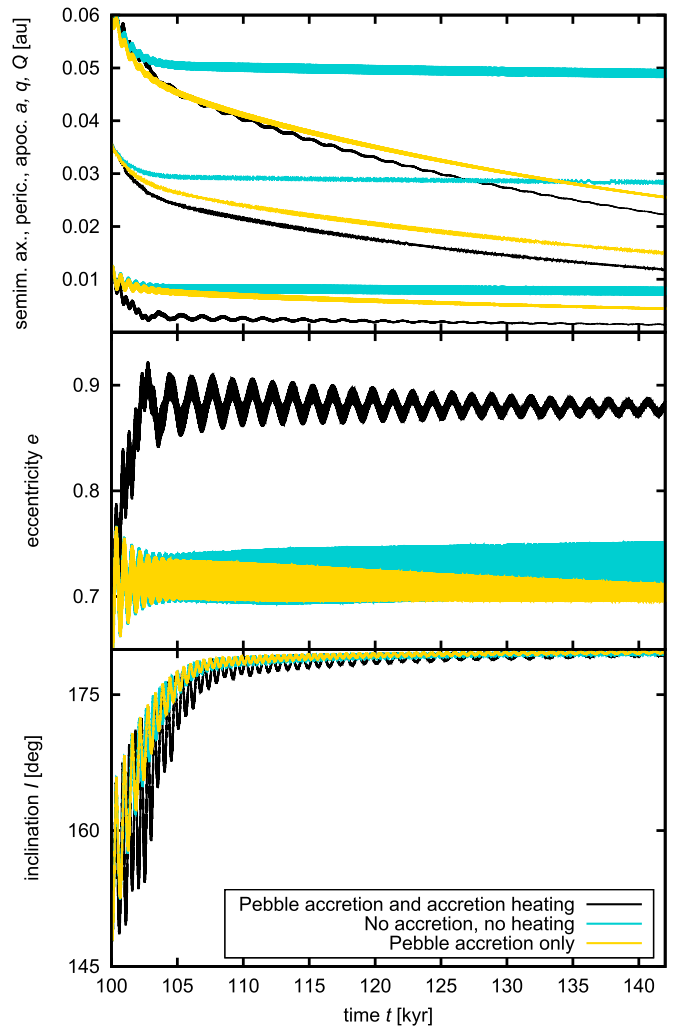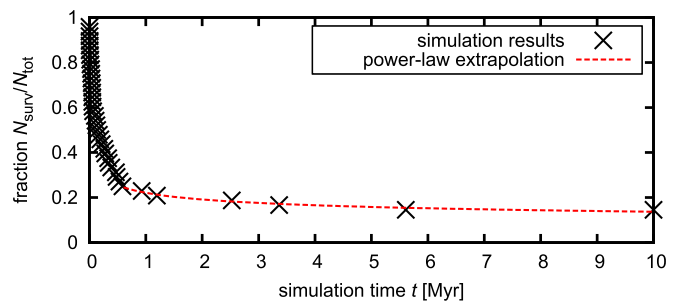
Figure 6. The temporal evolution of the orbital elements of the binary planet, namely the semimajor axis a (top), eccentricity e (middle), and inclination I (bottom). The color of the curves changes if different embryos become locked in the binary configuration during a three-body encounter (see Figure 5 for reference). The encounters can be recognized as sudden spikes and they typically lead to a sudden decrease of a and e. In the course of time, the binary becomes bound more tightly. The existence of the binary ends with a merger, marked by an arrow.

Figure 7. Stability test starting from the binary planet configuration corresponding to $t = 100$ kyr in Figure 6. In this test, the surrounding planetary embryos are removed. Therefore we study evolution of an isolated binary driven only by its interactions with the disk and not by close encounters. Three cases are shown: one with the complete RHD and two-fluid part of the model (black curve), one with pebble accretion but without accretion heating (gold curve), and one with neither pebble accretion nor heating (turquoise curve). Pebble accretion (i.e., mass growth) of the embryos generally causes the decrease in the semimajor axis. Accretion heating, on the other hand, is capable of pumping the eccentricity above the initial value.

classes. The more common first class comprises five systems (simulation numbers 5, 12, 28, 34, 37) in which one of the binary components undergoes an early collision (at about $\simeq 0.1$ Myr) with one of the remaining embryos while maintaining the binary configuration. The collision reduces the multiplicity of the system and changes the mass ratio of the binary components from $1/1$ to $2/1$. The stability of such systems is obvious from Figure 9 because eccentricities are only marginally excited and the planets do not undergo orbital crossings.

The less frequent second class of orbital architectures (simulation numbers 17 and 38) includes systems in which no collision occurred yet the binary managed to survive close encounters. Orbits of the single embryos in these simulations are moderately eccentric and have orbital crossings with the binary. It is very likely that these systems would reconfigure and the binary would dissolve when integrating for $t > 10$ Myr. However, we

Figure 8. The fraction of N-body integrations in which the binary planet survives until simulation time t. The crosses mark the results of our integrations; the dashed curve is a power-law fit that is used as an extrapolation for $t > 10$ Myr.
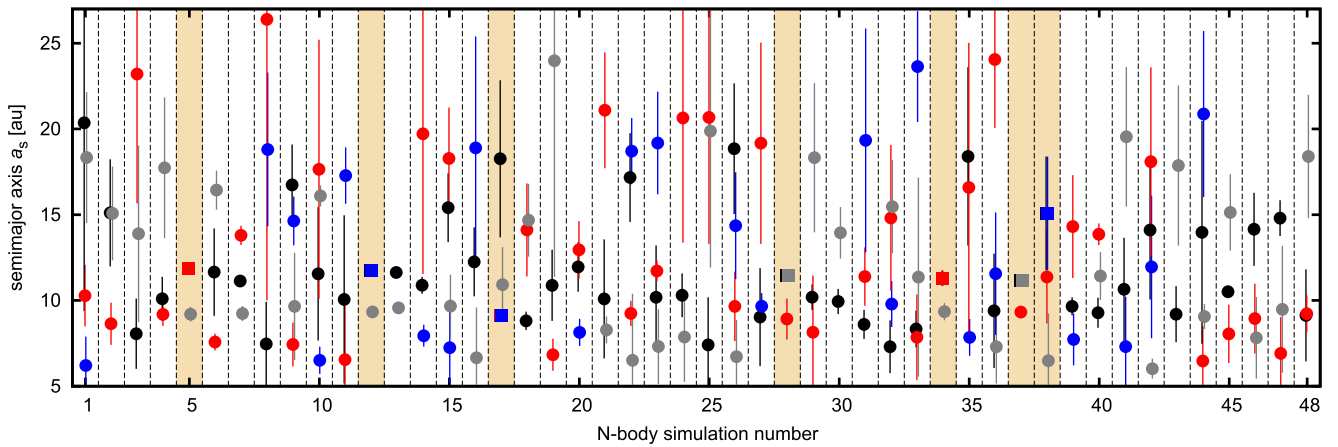
Figure 9. Orbital distribution of the planetary systems 10 Myr after removal of the disk. The horizontal axis shows the reference number of *N*-body simulations; individual cases are separated by the vertical dashed lines. The vertical axis shows the stellarcentric semimajor axis of planets displayed with symbols (the coloring is the same as in the previous figures). Single planets are marked by filled circles, binary planets are distinguished by filled squares (squares correspond to a_s of the binary barycenter). The systems that preserved the binary are also highlighted using a yellow background. The vertical bars of each symbol indicate the span of orbits from pericenter to apocenter (large bars correspond to eccentric orbits and smaller ones to more circular orbits).

believe that these two cases are accounted for by the power-law extrapolation when estimating f_{surv} for old systems.

3.8. Formation Efficiency

So far the analysis has been based on our nominal simulation. Although a broader study of the parametric space is difficult using RHD simulations, it is important to quantify how common it is for transients to become hardened and stabilized in three-body encounters. Also, it is desirable to test whether the result is sensitive to the choice of initial separations, embryo masses, and embryo multiplicity.

We perform four additional full RHD simulations in which we vary the initial conditions for embryos (the disk remains the same as in Section 3.1). Embryos start with different random longitudes, and inclinations are $I_s = I_0$. Two simulations (denoted I and II) are run with four embryos, each having $M_{em} = 3 M_\oplus$ again, but the innermost embryo is initially placed at $a_s = 6$ au and the remaining ones are spaced by 10 mutual Hill radii. Two simulations (denoted III and IV) include eight embryos with $M_{em} = 1.7 M_\oplus$, the innermost one being placed at $a_s = 5$ au and the others having initial separations of eight mutual Hill radii.

Simulations I and II cover 120 kyr of evolution. A common feature of these runs is a merger occurring relatively early (at $\simeq$40 kyr and $\simeq$51 kyr in simulations I and II, respectively), followed by a second merger (at $\simeq$81 kyr and $\simeq$94 kyr, respectively). Simulation III covers 180 kyr of evolution. There is a late violent sequence at $\simeq$150 kyr during which two mergers occur and three embryos are scattered out of the simulated part of the disk.

In simulations I–III, only transient binaries are formed. However, we detect one case of a hardened binary in simulation IV, which covers 120 kyr of evolution. The simulation also contains 190 transients compared to 65 cases found in our nominal simulation, which implies that the increased multiplicity of the system (eight embryos instead of four) logically increases the frequency of embryo encounters. Figure 10 shows the evolution of orbital elements of the binary configurations participating in binary hardening. First, a transient consisting of embryos 2 and 7 forms at about 122.5 kyr. After $\simeq$1 kyr, it undergoes a three-body encounter
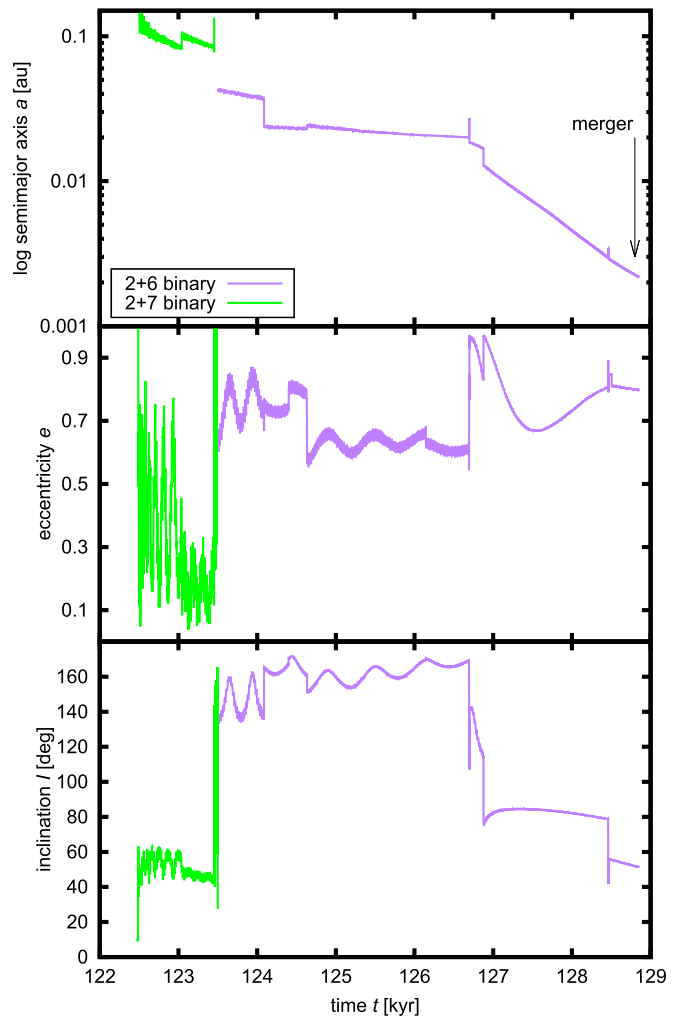
Figure 10. As in Figure 6, but for the binary configurations found in our additional simulation IV with eight embryos (initial $M_{em} = 1.7 M_\oplus$). The binary shown here undergoes similar evolution to that in Figure 6.

during which the configuration changes to embryos 2 and 6 and the semimajor axis of the binary decreases. Then the binary evolves for about 5 kyr due to pebble accretion and additional

three-body encounters. The secular rate of change of a is clearly related to the value of I, suggesting that the deposition of pebbles onto a prograde binary causes the separation to decrease faster than in a retrograde case. As in the nominal simulation, the binary separation shrinks until the binary merges.

Although the statistics of our five (one nominal and four additional) RHD simulations is still poor, we can nevertheless conclude that a binary planet with a considerable lifetime can form in at least some cases. We can also make a crude estimate of the formation efficiency f_{form}, which we define as the fraction of simulations in which a binary planet was formed and then hardened, obtaining $f_{form} \simeq 0.4$.

For simulations that formed such binaries, we also define the total time τ_{bp} for which the binary planet existed in the system (regardless of which embryos were bound). The binary in our nominal simulation existed for $\simeq 16\,kyr$ and the binary in simulation IV existed for $\simeq 6\,kyr$ in total. Taking the arithmetic mean of these two values, we obtain $\tau_{bp} \simeq 11\,kyr$.

4. Discussing Binary Planets

4.1. Model Complexity and Limitations

The choice of the RHD model was not a priori motivated by studying the formation of binary planets. The initial motivation was to check how the evolution described in Chrenko et al. (2017) changes if the orbits of embryos become inclined due to the vertical hot-trail effect (only the horizontal hot trail was modeled in Chrenko et al. 2017). We found binary planet formation as an unexpected yet natural outcome of the model.

It is possible that a less complex model could be applied to scan the parametric space, e.g., by N-body integrations. But although there are many state-of-the-art N-body models of migration in multiplanet systems with disks (e.g., Cossou et al. 2013, 2014; Izidoro et al. 2017), none of them (to our knowledge) identified the formation of binary planets. This suggests that there might be issues preventing binary planet formation in such models.

We demonstrated in Section 3.4 that hydrodynamic effects are important during the formation of transient binaries by two-body encounters. The pair of approaching embryos creates perturbations in the disk that differ from perturbations arising from isolated embryos. The prescriptions for the disk torques that are currently used in N-body models (Cresswell & Nelson 2008; Paardekooper et al. 2010, 2011; Fendyke & Nelson 2014) cannot account for such effects because they were derived from models containing a single embryo, not an interacting pair. Moreover, such prescriptions do not account for the thermal torque and hot-trail effect.

We point out that our RHD model has some limitations as well. First, although the grid resolution leads to numerical convergence of the migration rate for low-mass planets (see, e.g., Lega et al. 2014; Brož et al. 2018, for discussions of resolution), it is not tuned to resolve binary configurations with the smallest orbital separations well enough. However, looking at the turquoise curve in Figure 7 (i.e., the case without additional perturbers), the marginal change of orbital elements indicates a very low level of numerical dissipation, safely negligible over a typical binary lifetime during the disk phase. Second, the vertical hot trail cannot be implemented in our 2D model in a self-consistent way. 3D simulations would be required to assess the importance of the vertical dimension,

which we neglect here. Finally, the magnitude of the thermal torques depends on the thermal diffusivity and therefore on the opacity (Masset 2017). However, we used a single opacity prescription and it remains unclear whether the described effects work the same way, e.g., in a low-density disk undergoing photoevaporation.

4.2. Formation Mechanism

We found that two-body encounters of planetary embryos in the gas disk can establish transient binaries. A binary planet with a considerable lifetime can form from a transient by a three-body encounter that provides the necessary energy dissipation to make the pair more tightly bound. Here we discuss whether there are other mechanisms suitable for formation of binary planets.

An additional possibility exists during the reaccumulation phase after a large impact of two embryos approaching on initially unbound trajectories, as discussed by Ryan et al. (2014). But this situation is highly unlikely. Head-on collisions usually disrupt the protoplanets in such a way that the reaccumulation forms a large primary and a low-mass disk, from which a satellite can be assembled but not a binary companion. Only a special grazing geometry with a large impact parameter can be successful (Ryan et al. 2014) and it can only produce binaries with separations of a few planetary radii due to the angular momentum deficit of such an encounter.

Finally, planets can be captured in a binary configuration by means of tidal dissipation. Ochiai et al. (2014) studied the evolution of three hot Jupiters around a host star and discovered that binary gas giants can form in $\sim 10\%$ of systems that undergo orbital crossings.

4.3. Mass of the Binary

In our hydrodynamic simulations, the components of binaries have comparable masses of several $M_\oplus$ before they merge. But as we found in the follow-up gas-free N-body simulations, the system often stabilizes by a collision of one of the embryos with the binary. If the binary survives the collision, the mass ratio of the components increases to $2/1$. Therefore it seems that, if born from a population of equal-mass embryos (as obtained in the oligarchic growth scenarios), binary planets would preferentially exist with the component mass ratio $1/1$ or $2/1$. This aspect of our model is related to the choice of the initial embryo masses and is of course too simplified to capture the outcome of models where accretion creates a range of embryo masses.

Although simulations with gas accretion onto the planets are beyond the scope of our paper, we believe that runaway accretion of gas onto the binary would disrupt it. We thus expect that the binary planets formed in three-body encounters cannot exceed the masses of giant planet cores. This could be ensured by the mechanism of pebble isolation (Lambrechts et al. 2014; Bitsch et al. 2018) or simply because binaries could form late, just before dispersal of the gas disk. However, it is possible that binary giant planets form later by the mechanism of tidal capture (Ochiai et al. 2014).

4.4. Tidal Evolution

Orbital evolution due to tidal dissipation is without doubt an important factor for the stability of binary planets. However, it

is difficult to assess the tidal effects at this stage because there are many unknown parameters. A large uncertainty lies in the parameter k_2/Q, where k_2 is the degree 2 Love number and Q is the tidal quality factor (e.g., Harris & Ward 1982). These parameters reflect the interior structure and thus they depend on the planetary composition (water-rich versus silicate-rich) and state (cold versus magma worlds), the latter of which changes on an uncertain timescale. Moreover, our model treats the planets as point-mass objects, and therefore we have no information about their rotation, which is important to determine the level of spin–orbital synchronicity. Additionally, similar masses of the binary components and their (possibly) retrograde and highly eccentric orbit make the analysis of tides even more complicated. For all these reasons, the model of tidal evolution of a binary planet should be sufficiently complex and should account for the internal structure and rheology (e.g., Boué et al. 2016; Walterová & Běhounková 2017).

4.5. Occurrence Rate and Observability

We define the occurrence rate of binary planets f_{bp} as the fraction of planetary systems that are expected to contain at least one binary planet hardened by three-body encounters. An order-of-magnitude estimate can be obtained by dividing the timescale $\tau_{bp} \simeq 10^4$ yr for which these binary planets are typically present in our simulations (Section 3.8) by the lifetime of protoplanetary disks $\tau_{disk} \simeq 10^7$ yr (e.g., Fedele et al. 2010), correcting for the formation efficiency $f_{form} \simeq 0.4$ (Section 3.8) and for the fraction of the emerging planetary systems f_{stab} in which the binary planet can survive after dispersal of the gas disk (Section 3.7). This leads to

$$f_{bp} = f_{form} \frac{\tau_{bp}}{\tau_{disk}} f_{stab}. \tag{12}$$

We quantify two characteristic values for young planetary systems (using $f_{stab,10\,Myr} \simeq 0.15$) and for old planetary systems (using $f_{stab,4.5\,Gyr} \simeq 0.04$), leading to $f_{bp,10\,Myr} \simeq 6 \times 10^{-5}$ and $f_{bp,4.5\,Gyr} \simeq 2 \times 10^{-5}$. In other words, one out of $\simeq (2\text{–}5) \times 10^4$ planetary systems should contain a binary planet formed by two- and three-body encounters.

We emphasize that the estimate is highly uncertain because it is inferred from a small number of tests. Moreover, our simulations cover only a small region of the protoplanetary disk, the evolution timescale is still short compared to the disk's lifetime, and the number of embryos is relatively low. Last but not least, our estimate assumes that binaries only form by the processes identified in this work.

As pointed out in Section 1, the estimated occurrence rate should motivate a systematic search for binary planets in the observational data. For example, binary planets should be detectable by the Hunt for Exomoons with *Kepler* (HEK) project (Kipping et al. 2012). The sensitivity of this survey is $\simeq 40\%$ for binaries with Pluto–Charon mass ratios (Kipping et al. 2015).

4.6. Role in Planetary Systems

The possible existence of binary planets opens new avenues in planetary sciences. A study of long-term orbital dynamics and stability of binaries in various systems is needed (e.g., Donnison 2010), including an assessment of their tidal evolution. Binary planets are challenging for hydrodynamic modeling as well. Local high-resolution simulations of

interactions with the disk, pebble accretion, pebble isolation (e.g., Bitsch et al. 2018), and gas accretion (e.g., Lambrechts & Lega 2017) should be performed for binary planets (preferably in 3D) to understand the impact of these processes in detail.

In this paper, we reported various fates of binary planets (considering the set of gas-free *N*-body simulations). Frequently, one of the binary components underwent a collision with an equally large impactor, or the binary merged. The merger of the binary planet is a process that should be investigated (e.g., by the smoothed-particle hydrodynamics (SPH) method, Jutzi 2015).

A merger can occur in a situation when the binary orbit is inclined with respect to the global orbital plane, and the resulting body would then retain the initial angular momentum of the binary, forming a planet (or a giant planet core) with an angular tilt of the rotational axis. It might be worth investigating the relation of such an event to the origin of Uranus.

Moreover, the collision of the binary components would statistically occur at high impact angles. It is interesting that such impact angles and similar masses of the target and the impactor (although on unbound trajectories) were also used for a successful explanation of the impact origin of the Earth–Moon system (Canup 2012).

5. Conclusions

By means of 2D radiation hydrodynamic simulations with 3D planetary orbits, we described the formation of binary planets in a system of migrating super-Earths. A key ingredient of the model is the vertical hot-trail effect (Eklund & Masset 2017), which was incorporated by reducing the efficiency of the prescription for inclination damping (Tanaka & Ward 2004). We also accounted for the pebble disk, pebble accretion, and accretion heating, which naturally produces the horizontal hot-trail effect, providing excitation of eccentricity (Chrenko et al. 2017).

When convergent migration drives the planetary embryos together, the geometry of their encounters allows for vertical perturbations owing to the non-zero inclinations. The orbits become vertically stirred and dynamically hot, reaching inclinations up to $\simeq 2°$.

Numerous transient binary planets form during the simulations by gas-assisted two-body encounters but such transients dissolve quickly. Binary planets with longer lifetimes $\sim 10^4$ yr form when a transient undergoes a three-body encounter with a third embryo. During this process of binary hardening, energy is removed from the binary orbit and the separation of components decreases. Also, three-body encounters often reconfigure the binary when one of the components swaps places with the encountered embryo. The existence of hardened binaries in our simulations typically ends with a merger of its components, which forms a giant planet core.

The role of the gas disk in binary planet formation is twofold. In two-body encounters, the disk can dissipate orbital energy of the embryos, thus aiding the gravitational capture. The dissipation is provided when the embryos cross a shared spiral arm. In three-body encounters, the disk torques hold the embryos closely packed and the hot-trail effect maintains the eccentricities and inclinations excited, increasing the probability that a transient will encounter another embryo before it dissolves.

We conducted numerical experiments to test the stability and evolution of binary planets in cases when pebble accretion is halted, or accretion heating is inefficient, or the disk dissipates. We found that pebble accretion causes a secular decrease of a of the binary whereas e increases due to the hot-trail effect.

For the binary to survive after dispersal of the disk, it is required that the surrounding embryos are removed or reconfigured dynamically. Quite often, a stable configuration is achieved when one of the components of the surviving binary undergoes a merger with another embryo, increasing the binary mass ratio from approximately $1/1$ to $2/1$.

We roughly estimated the expected fraction of planetary systems with binary planets to be $f_{\rm bp} \simeq (2\text{–}6) \times 10^{-5}$, where the upper limit holds for young planetary systems and the lower limit holds for 4.5 Gyr old systems. In other words, a binary planet should be present in one planetary system out of $\simeq (2\text{–}5) \times 10^4$.

One can think of many new applications that the possible existence of binary planets brings. First, although binary planets have yet to be discovered, our estimate of their occurrence rate is encouraging for future observations. Second, the hydrodynamic interactions of binary planets with the disk may be different from those of a single planet and are worth investigating, preferably in 3D. Third, collisional models for planetary bodies that usually focus on unbound trajectories should also investigate colliding binaries to assess the possible outcomes.

ORCID iDs

Ondřej Chrenko ⓘ https://orcid.org/0000-0001-7215-5026
Miroslav Brož ⓘ https://orcid.org/0000-0003-2763-1411
David Nesvorný ⓘ https://orcid.org/0000-0002-4547-4301

References

Araujo, R. A. N., Winter, O. C., Prado, A. F. B. A., & Vieira Martins, R. 2008, MNRAS, 391, 675
Astakhov, S. A., Lee, E. A., & Farrelly, D. 2005, MNRAS, 360, 401
Baillié, K., & Charnoz, S. 2014, ApJ, 786, 35
Baruteau, C., & Masset, F. 2008, ApJ, 672, 1054
Bell, K. R., & Lin, D. N. C. 1994, ApJ, 427, 987
Benéz-Llambay, P., Masset, F., Koenigsberger, G., & Szulágyi, J. 2015, Natur, 520, 63
Benéz-Llambay, P., & Pessah, M. E. 2018, ApJL, 855, L28
Ben-Jaffel, L., & Ballester, G. E. 2014, ApJL, 785, L30
Bennett, D. P., Batista, V., Bond, I. A., et al. 2014, ApJ, 785, 155
Birnstiel, T., Klahr, H., & Ercolano, B. 2012, A&A, 539, A148
Bitsch, B., Crida, A., Morbidelli, A., Kley, W., & Dobbs-Dixon, I. 2013, A&A, 549, A124
Bitsch, B., Morbidelli, A., Johansen, A., et al. 2018, A&A, 612, A30
Boué, G., Correia, A. C. M., & Laskar, J. 2016, CeMDA, 126, 31
Brown, M. E., van Dam, M. A., Bouchez, A. H., et al. 2006, ApJL, 639, L43
Brož, M., Chrenko, O., Nesvorný, D., & Lambrechts, M. 2018, arXiv:1810.03385
Brozović, M., Showalter, M. R., Jacobson, R. A., & Buie, M. W. 2015, Icar, 246, 317
Canup, R. M. 2011, AJ, 141, 35
Canup, R. M. 2012, Sci, 338, 1052
Chiang, E. I., & Goldreich, P. 1997, ApJ, 490, 368
Chrenko, O., Brož, M., & Lambrechts, M. 2017, A&A, 606, A114
Christy, J. W., & Harrington, R. S. 1978, AJ, 83, 1005
Cordeiro, R. R., Martins, R. V., & Leonel, E. D. 1999, AJ, 117, 1634
Cossou, C., Raymond, S. N., Hersant, F., & Pierens, A. 2014, A&A, 569, A56
Cossou, C., Raymond, S. N., & Pierens, A. 2013, A&A, 553, L2
Cresswell, P., Dirksen, G., Kley, W., & Nelson, R. P. 2007, A&A, 473, 329
Cresswell, P., & Nelson, R. P. 2008, A&A, 482, 677
Crida, A., Sándor, Z., & Kley, W. 2008, A&A, 483, 325
D'Angelo, G., Henning, T., & Kley, W. 2003, ApJ, 599, 548
de Val-Borro, M., Edgar, R. G., Artymowicz, P., et al. 2006, MNRAS, 370, 529
Donnison, J. R. 2010, MNRAS, 406, 1918
Eklund, H., & Masset, F. S. 2017, MNRAS, 469, 206
Erikson, A., Santerne, A., Renner, S., et al. 2012, A&A, 539, A14
Fedele, D., van den Ancker, M. E., Henning, T., Jayawardhana, R., & Oliveira, J. M. 2010, A&A, 510, A72
Fendyke, S. M., & Nelson, R. P. 2014, MNRAS, 437, 96
Fraser, W. C., Bannister, M. T., Pike, R. E., et al. 2017, NatAs, 1, 0088
Giuppone, C. A., Benéz-Llambay, P., & Beaugé, C. 2012, MNRAS, 421, 356
Goldreich, P., Lithwick, Y., & Sari, R. 2002, Natur, 420, 643
Han, C. 2008, ApJ, 684, 684
Harris, A. W., & Ward, W. R. 1982, AREPS, 10, 61
Heller, R. 2014, ApJ, 787, 14
Heller, R. 2018, A&A, 610, A39
Hills, J. G. 1975, AJ, 80, 809
Hills, J. G. 1990, AJ, 99, 979
Hippke, M. 2015, ApJ, 806, 51
Hubeny, I. 1990, ApJ, 351, 632
Izidoro, A., Ogihara, M., Raymond, S. N., et al. 2017, MNRAS, 470, 1750
Jutzi, M. 2015, P&SS, 107, 3
Kipping, D. M. 2009, MNRAS, 392, 181
Kipping, D. M., Bakos, G. Á, Buchhave, L., Nesvorný, D., & Schmitt, A. 2012, ApJ, 750, 115
Kipping, D. M., Schmitt, A. R., Huang, X., et al. 2015, ApJ, 813, 14
Klahr, H., & Kley, W. 2006, A&A, 445, 747
Kley, W. 1989, A&A, 208, 98
Kley, W., Bitsch, B., & Klahr, H. 2009, A&A, 506, 971
Kley, W., & Crida, A. 2008, A&A, 487, L9
Lambrechts, M., & Johansen, A. 2012, A&A, 544, A32
Lambrechts, M., & Johansen, A. 2014, A&A, 572, A107
Lambrechts, M., Johansen, A., & Morbidelli, A. 2014, A&A, 572, A35
Lambrechts, M., & Lega, E. 2017, A&A, 606, A146
Laughlin, G., & Chambers, J. E. 2002, AJ, 124, 592
Lee, M. H., & Peale, S. J. 2006, Icar, 184, 573
Lega, E., Crida, A., Bitsch, B., & Morbidelli, A. 2014, MNRAS, 440, 683
Lega, E., Morbidelli, A., & Nesvorný, D. 2013, MNRAS, 431, 3494
Lewis, K. M., Ochiai, H., Nagasawa, M., & Ida, S. 2015, ApJ, 805, 27
Liebig, C., & Wambsganss, J. 2010, A&A, 520, A68
Marchis, F., Descamps, P., Baek, M., et al. 2008, Icar, 196, 97
Marchis, F., Hestroffer, D., Descamps, P., et al. 2006, Natur, 439, 565
Margot, J. L., Nolan, M. C., Benner, L. A. M., et al. 2002, Sci, 296, 1445
Masset, F. 2000, A&AS, 141, 165
Masset, F. S. 2002, A&A, 387, 605
Masset, F. S. 2017, MNRAS, 472, 4204
Masset, F. S., & Velasco Romero, D. A. 2017, MNRAS, 465, 3175
McKinnon, W. B., Stern, S. A., Weaver, H. A., et al. 2017, Icar, 287, 2
Menou, K., & Goodman, J. 2004, ApJ, 606, 520
Mihalas, D., & Weibel Mihalas, B. 1984, Foundations of Radiation Hydrodynamics (New York: Oxford Univ. Press)
Morbidelli, A., & Nesvorný, D. 2012, A&A, 546, A18
Müller, T. W. A., Kley, W., & Meru, F. 2012, A&A, 541, A123
Nesvorný, D., Youdin, A. N., & Richardson, D. C. 2010, AJ, 140, 785
Noll, K. S., Grundy, W. M., Stephens, D. C., Levison, H. F., & Kern, S. D. 2008, Icar, 194, 758

Ochiai, H., Nagasawa, M., & Ida, S. 2014, ApJ, 790, 92
Ormel, C. W., & Klahr, H. H. 2010, A&A, 520, A43
Paardekooper, S.-J., Baruteau, C., Crida, A., & Kley, W. 2010, MNRAS, 401, 1950
Paardekooper, S.-J., Baruteau, C., & Kley, W. 2011, MNRAS, 410, 293
Paardekooper, S.-J., & Mellema, G. 2008, A&A, 478, 245
Papaloizou, J. C. B., & Larwood, J. D. 2000, MNRAS, 315, 823
Pierens, A. 2015, MNRAS, 454, 2003
Pierens, A., Cossou, C., & Raymond, S. N. 2013, A&A, 558, A105
Pravec, P., Scheirich, P., Kušnirák, P., et al. 2006, Icar, 181, 63
Pravec, P., Scheirich, P., Vokrouhlický, D., et al. 2012, Icar, 218, 125
Rein, H., & Liu, S.-F. 2012, A&A, 537, A128
Rein, H., & Spiegel, D. S. 2015, MNRAS, 446, 1424
Richardson, D. C., & Walsh, K. J. 2006, AREPS, 34, 47

Ryan, K., Nakajima, M., & Stevenson, D. J. 2014, AAS Meeting, 46, 201.02
Scheeres, D. J., Fahnestock, E. G., Ostro, S. J., et al. 2006, Sci, 314, 1280
Simó, C., & Stuchi, T. J. 2000, PhyD, 140, 1
Simon, A., Szatmáry, K., & Szabó, G. M. 2007, A&A, 470, 727
Simon, A. E., Szabó, G. M., Kiss, L. L., & Szatmáry, K. 2012, MNRAS, 419, 164
Sonnett, S., Mainzer, A., Grav, T., Masiero, J., & Bauer, J. 2015, ApJ, 799, 191
Tanaka, H., & Ward, W. R. 2004, ApJ, 602, 388
Teachey, A., Kipping, D. M., & Schmitt, A. R. 2018, AJ, 155, 36
Veillet, C., Parker, J. W., Griffin, I., et al. 2002, Natur, 416, 711
Walker, A. R. 1980, MNRAS, 192, 47P
Walsh, K. J., Richardson, D. C., & Michel, P. 2008, Natur, 454, 188
Walterová, M., & Běhounková, M. 2017, CeMDA, 129, 235
Youdin, A. N., & Lithwick, Y. 2007, Icar, 192, 588